RAPID COMMUNICATIONS IN MASS SPECTROMETRY
Rapid Commun. Mass Spectrom. **12**, 1253–1260 (1998)

Postionization of Molecules Desorbed from Surfaces by keV Ion Bombardment with Femtosecond Laser Pulses

Kenneth F. Willey, Vasil Vorsa, Robert M. Braun and Nicholas Winograd*

Department of Chemistry, The Pennsylvania State University, 184 Materials Research Institute Building, University Park, PA 16802, USA

We report the use of femtosecond laser photoionization of sputtered neutral molecules to enhance the sensitivity of detection and to improve the prospects for molecule-specific imaging experiments. Results are presented for patterned metal oxides, polycyclic aromatic hydrocarbons and several amino acids. In addition to increased signal levels, we find that fs photoionization generally yields simpler mass spectra than the corresponding SIMS spectra, although considerable fragmentation is observed in both cases. © **1998 John Wiley & Sons, Ltd.**

Received 24 April 1998; Revised 22 July 1998; Accepted 24 July 1998

Recent advances in liquid metal ion gun technology have improved chemical imaging capabilities by increasing the spatial resolution to sub-micron values. This configuration, however, places an increased demand on the detection efficiency for desorbed species due to the smaller number of available molecules. During the ion bombardment process, neutral species as well as positive and negative ions are desorbed. In general the neutral component is the most intense, often by several orders of magnitude. Therefore, efficient analysis of the neutral species would potentially yield much more signal, when compared to only desorbed ion detection. An additional advantage to probing neutral species is that the desorption yield is less dependent on the electronic environment[1] which allows for a more accurate representation of surface composition.

Initial studies in our laboratory have utilized nanosecond laser pulses for postionization experiments.[2–4] This approach has proven successful in the surface analysis of desorbed atomic and molecular species, with detection limits achieved in the low ppt levels when incorporating resonance enhanced multiphoton ionization.[5] Fragmentation, however, is a concern when photoionizing molecular systems through a multiphoton ionization (MPI) process. At each step in the absorption ladder, there is a competition between the absorption of additional photons or de-excitation through competing processes such as internal conversion, intersystem crossing and predissociation which may lead to the loss of molecular ion signal. Currently, two alternative schemes are being explored as possible methods to bypass these relaxation channels in postionization. One is the use of vacuum ultraviolet (VUV) excitation[6] and the other is the use of ultrashort laser pulses.

Recent studies in our laboratory have focused on incorporating high power femtosecond laser pulses to enhance signal levels in postionization experiments. The enhanced absorption rates generated by these pulses make it possible to 'outrun' the neutral fragmentation channels, which are prevalent when employing nanosecond excitation of molecular species. Furthermore, the high photon flux, accompanying femtosecond excitation, dramatically increases the probability of non-resonant processes. Ledingham and co-workers have shown the promise of ultra-short pulse excitation in recent gas phase studies.[7,8] They report a dramatic decrease in the degree of fragmentation when switching from nanosecond to femtosecond pulses in the photoionization of NO_2.[8] A similar trend has been reported for the metal carbonyls, which fragment to bare metal atoms in nanosecond MPI experiments.[9,10] Other examples illustrating the generation of strong molecular ion signals when using femtosecond excitation have been reported.[11,12] Femtosecond postionization studies showing a significant reduction in the degree of fragmentation when compared to nanosecond excitation have been reported.[13–15] For example, Benninghoven and co-workers report ionization efficiencies for producing intact molecular ions from sinapinic acid and tryptophan are comparable to those found for atomic photoionization.[14]

In this paper we discuss the pertinent experimental factors associated with postionization of desorbed neutral molecules and how they relate to chemical imaging of surfaces. A detailed description of the Ti:sapphire femtosecond laser system is provided to present the reader with the technology required to generate ultra-short pulses. Moreover, we discuss some of the photophysics issues that govern ion formation and describe possible photoionization mechanisms that become operative when high power femtosecond pulse excitation is employed.

EXPERIMENTAL

The details of the time-of-flight secondary ion mass spectrometry (TOF-SIMS) apparatus and its imaging capabilities have been described previously[4,16] and only the details particular to these studies are presented here. Leucine, phenylalanine and pyrene butyric acid were

*Correspondence to: N. Winograd, Department of Chemistry, The Pennsylvania State University, 184 Materials Research Institute Building, University Park, PA 16802, USA.
Contract/grant sponsor: National Science Foundation.
Contract/grant sponsor: National Institutes of Health.

CCC 0951–4198/98/181253–08 $17.50

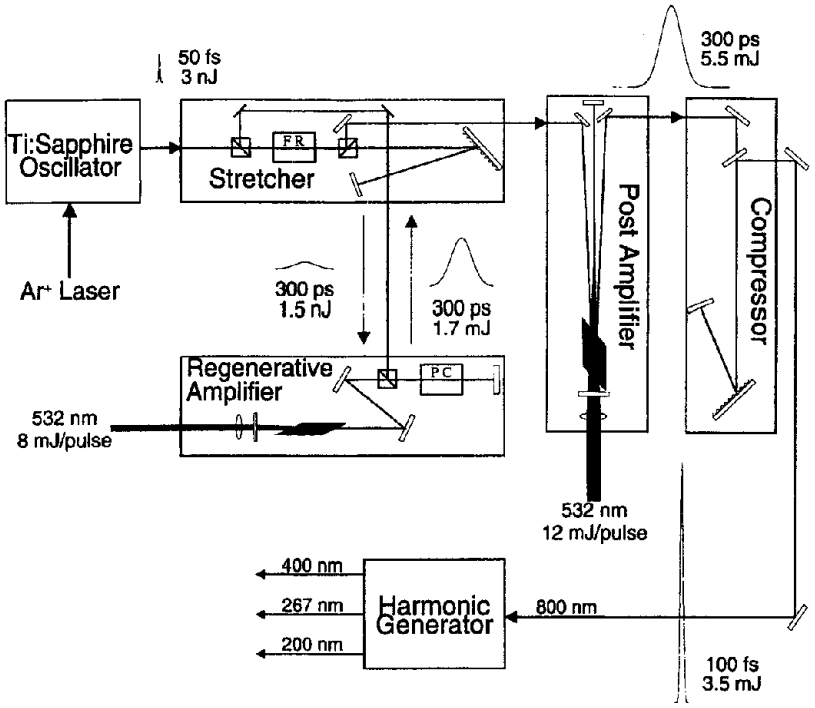

Figure 1. Schematic diagram of the Ti:sapphire femtosecond laser system incorporating two stages of amplification and a harmonic generator.

purchased from Sigma (purity >99%) and used without further purification. Each amino acid was dissolved to a concentration of $\sim 10^{-2}$ M in a 50/50 solution of HPLC grade water and absolute ethanol. The solution was then pipetted onto a clean Si wafer and allowed to dry before analysis. Pyrene butyric acid was physisorbed onto 40–100 μm silver beads by placing the silver beads in a $\sim 10^{-2}$ M solution of pyrene butyric acid in absolute ethanol for 24 hours. The solution was then decanted and the beads were allowed to dry before placing them onto a clean Si wafer for analysis. Molecules terminated with a carboxylic acid have been shown to self assemble onto silver oxide surfaces at concentrations of 10^{-4} M.[17] Higher concentrations were utilized here to ensure the physisorption of pyrene butyric acid onto the silver beads.

The samples are cooled to approximately 190 K in the analysis chamber to minimize sublimation, which can lead to substantial background signal.[4] A highly focused beam of 25 keV Ga^+ ions, from a Ga^+ liquid metal gun,[16] impinges on the sample surface inducing desorption of atomic and molecular species. The sample stage is held at ground potential prior to ion bombardment, which ensures that the ion beam raster on the surface is identical for the analysis of neutral and charged species. Ions are extracted directly into the reflectron based TOF mass analyzer by pulsing the sample stage shortly after ion bombardment. In postionization experiments, secondary ions formed during the sputtering process are removed by pulsing the stage negative for 50 ns following ion bombardment and by biasing the reflectron at a lower potential (~100 V) than the sample. Postionized species are extracted into the reflectron mass analyzer by applying a positive potential to the sample stage prior to laser interaction.

Figure 1 depicts the Ti:sapphire laser system[18–20] with the post-amplification stage (Clark-MXR)[21] used in these experiments. The self-modelocked Ti:sapphire oscillator, pumped by the 3 W output of an Ar ion laser (all lines), produces an 800 nm, 100 MHz, 3 nJ pulse train with ~50 fs pulse duration. Self-modelocking is generated by the Kerr lens effect.[22] A beam splitter redirects a portion (i.e. 4%) of the output beam to a photodiode, which triggers the Pockels cell driver. The remaining output is directed into the stretcher where the pulses are stretched to ~300 ps by multiple passes on a single grating before being sent through a Faraday isolator and into the Ti:sapphire regenerative amplifier. The amplifier is pumped with 8 W of the 532 nm output of an intracavity frequency doubled Nd:YAG laser. The regenerative amplifier and Nd:YAG laser are triggered at a repetition rate of 1 kHz set by the Pockels cell driver. The seed pulse inside the regenerative amplifier is allowed to build up gain by multiple round trips through the Ti:sapphire crystal before extraction from the cavity. The seed pulse is amplified over six orders of magnitude to ~1.7 mJ. The output beam is then directed back through the Faraday isolator and into the post amplifier. Further amplification to 5.5 mJ/pulse is achieved by four passes through a Ti:sapphire rod, which is pumped with 12 W at 532 nm from a second Nd:YAG laser. Finally, the beam is directed into a compressor where multiple passes on a single grating compress the amplified pulses to ~100 fs. The final output consists of an 800 nm, 1 kHz pulse train with each pulse containing 3.5 mJ of energy.

The output from this laser system can be frequency doubled, tripled or quadrupled to produce 400, 267 and 200 nm, respectively. The 400 nm beam is generated by passing the unfocused fundamental beam through a $12 \times 12 \times 1$ mm type I BBO crystal cut at $\theta = 29°$. Following the doubling process, the 800 nm and 400 nm beams are separated with a dichroic mirror and the polarization of the residual 800 nm beam is rotated 90° with a half-wave plate so that it is parallel to that of the 400 nm beam. The third harmonic (267 nm) is produced by

spatially and temporally combining these two beams in a $12 \times 12 \times 0.6$ mm type I BBO crystal cut at $\theta = 44°$. The time lag introduced by the dissimilar group velocity dispersions of the two beams traveling through the doubling crystal is compensated for by an optical delay line in the 800 nm path. The fourth harmonic (200 nm) is generated by spatially and temporally combining 267 and 800 nm beams in a $10 \times 10 \times 0.3$ mm type I BBO crystal cut at $\theta = 65°$. Poor beam quality of the 800 nm beam, after the doubling and tripling processes, requires that a portion (i.e. 10–20 %) of the input beam be split off prior to harmonic generation and used in this step. A second delay line in the 800 nm beam path is used to achieve temporal overlap of the two beams in the fourth harmonic crystal. The pulse energies obtained at 400, 267 and 200 nm are 1200, 450 and 30 μJ, respectively.

The harmonics are separated and directed into the analysis chamber with the use of dichroic mirrors. An upper limit of 230 fs has been measured for the 267 nm beam by cross-correlation with the 800 nm beam. The cross-correlation width was obtained by measuring the ion signal arising from short-lived molecular states as a function of temporal overlap between the 267 nm and 800 nm laser pulses. Using the same cross-correlation method an upper limit of 400 fs has been measured for the 200 nm. The pulse width of the second harmonic has not been measured directly, but should be no greater than that of the third harmonic. The laser spot size and position over the sample is controlled by movement of a 30 cm focal length CaF_2 lens mounted on a x, y, z manipulator outside the chamber. By changing the laser pulse energy and spot size, the laser intensity (measured in W/cm^2) in the extraction region may be varied over several orders of magnitude. The procedure utilized to estimate the beam area at the interaction region has been reported previously.[15]

The mass resolution of a reflectron-based TOF instrument in SIMS experiments, is largely determined by the duration of the gun pulse. This places an upper limit on the gun pulse duration that may be used and still obtain the mass resolving power to distinguish between pure organics and metal containing species. The time period in which ions are created in postionization experiments is defined by the duration of the laser pulse. Here, the mass resolution is governed by the ability of the reflectron to compensate for the initial velocity dispersion of desorbed neutral molecules and energy spread introduced by the spatial distribution across the laser beam. In postionization studies, much longer gun pulses may be utilized which correspond to larger ion doses at the sample per cycle. Larger doses directly translate into shorter acquisition times. The upper limit for the gun pulse duration, approximately 500 ns, maximizes the overlap between the laser beam and the neutral desorption flux.

Desorbed ions and photoionized neutral molecules are extracted into a time-of-flight tube where they are separated according to mass by a reflectron mass analyzer before striking a dual microchannel plate detector. The output signal is sent to a PC computer where mass spectra and chemical images are processed. We currently incorporate both digital and analog detection schemes. The digital scheme consists of a multi-hit time-to-digital converter (TDC) with a 1 ns sampling rate (EG&G Instruments, Signal Recovery). Experiments requiring analog detection utilize a transient digitizer with 2 ns sampling rate (Signatec, Inc.) is utilized.

Ion formation and photoionization mechanisms

Enhanced detection sensitivity in ion desorption experiments using postionization has been realized by incorporating nanosecond laser systems.[2–4] However, these lasers are limited to repetition rates of less than 100 Hz, which makes the use of these lasers in imaging experiments problematic. Advances in laser technology have made it possible to obtain high power sub-100 femtosecond laser pulses at kHz repetition rates. At high laser intensities, coherent processes become significant, thus making it possible to photoionize atoms and molecules through high order multiphoton non-resonant mechanisms. The photophysics involved in laser excitation of atoms is generally straightforward, while for molecular systems, the process is much more complicated. As mentioned earlier, a competition between de-excitation (i.e. internal conversion, intersystem crossing and predissociation) and the absorption of an additional photon occurs at each step in the absorption ladder for molecules. De-excitation through these channels leads to a decrease in molecular ion signal. The high photon flux accompanying ultra-short laser pulses produces absorption rates that are faster or of the same order with these competing processes. That is, an additional photon is absorbed before the excited state undergoes a transformation. When the absorption rate is high enough, this process continues until an ion is formed.

The absorption process is not necessarily terminated following the formation of an ion, however. Additional photons may be absorbed which may lead to dissociation of the ion. At low laser intensities, photoionization can best be characterized by a multiphoton process, which is governed by perturbation theory.[23] As the laser intensity approaches 10^{12} W/cm^2, ac-Stark effects become important which leads to a shifting and broadening of resonances.[24] At even higher laser intensities, the photoionization process enters a semi-quantum mechanical regime. The electric field generated by the laser pulse distorts the potential surface such that the barrier to ionization is suppressed. At these laser intensities, the probability of a valence electron tunneling through the barrier becomes significant. The unitless Keldysh parameter γ is used to distinguish between a MPI and tunneling ionization (TI) regime:[25,26]

$$\gamma = \omega(2m_e IP)^{1/2}/eE_0 \qquad (1)$$

in SI units, where ω is the angular frequency of the laser, m_e and e are the mass and charge of the electron, IP is the ionization potential and E_0 is the electric field strength of the laser radiation. MPI is believed to occur when $\gamma > 5$, while at values of $\gamma < 0.5$ TI is thought to dominate.[27] As can be seen by evaluating Eqn (1), TI occurs at low frequencies (longer wavelengths) where the photon order for MPI is high. At intermediate values of γ, it becomes difficult to distinguish between the two competing ionization regimes.

At yet higher laser intensities, the electric field suppresses the barrier to a point where the electron is free to escape. This process, known as barrier suppression ionization (BSI),[28,29] is defined by the critical laser intensity (i.e. I_{th}) required to suppress the one-dimensional Coulombic potential to a level that a bound valence electron can escape without tunneling through the barrier. This threshold value is

$$I_{th}(\mathrm{W/cm^2}) = 4.00 \times 10^9 IP^4(\mathrm{eV})/Z^2, \qquad (2)$$

where Z is the charge state produced on the ion. The

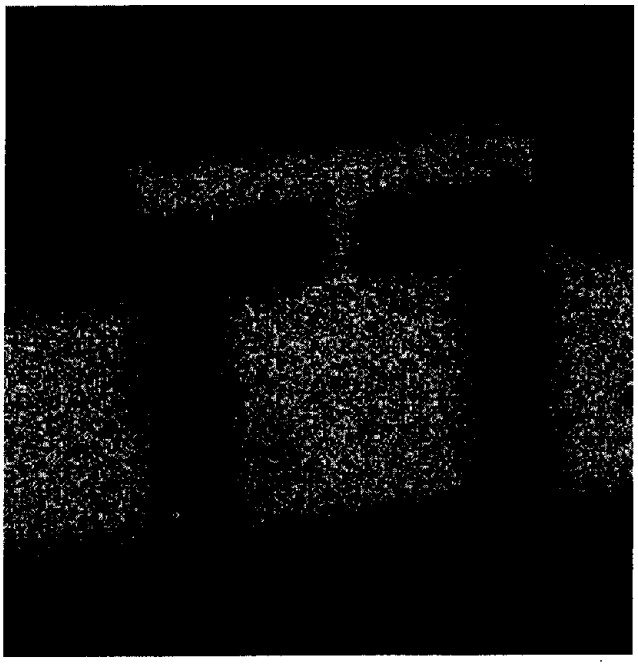

Figure 2. Postionization image of TiO^+ desorbed from an integrated circuit on a silicon substrate using 30 ns (1 nA) ion gun pulses with 5 shots per pixel (1.2×10^{11} Ga^2 ions/cm^2). The TiO molecules are ionized with 800 nm, 100 fs laser pulses at a laser power of 1.4×10^{14} W/cm^2. The 256 pixel × 256 pixel image was collected from a 225 μm × 225 μm area.

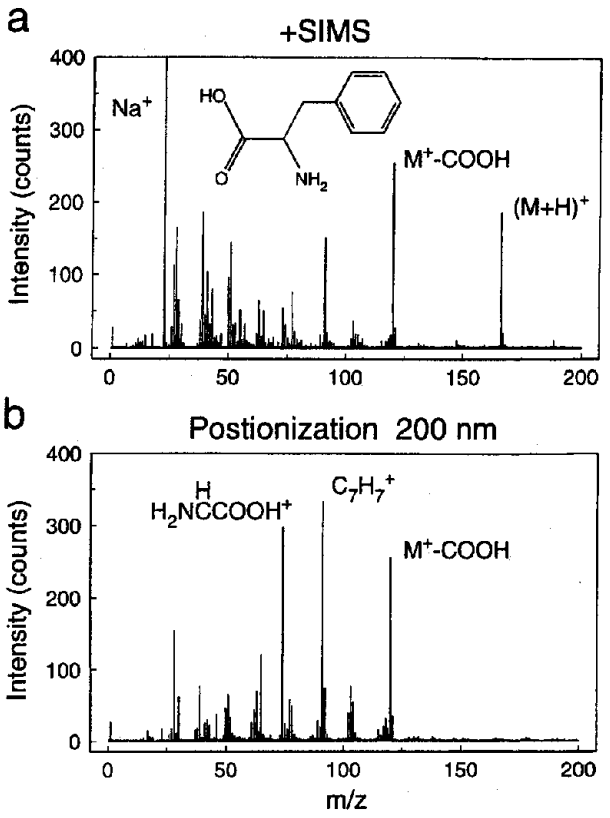

Figure 3. TOF spectra of phenylalanine on Si. (a) +SIMS (b) femtosecond-postionization at 200 nm at 8.2×10^{10} W/cm^2.

tunneling and barrier suppression ionization models were developed for atoms and have shown excellent agreement in photoionization experiments.[26–29] Furthermore, these models have successfully described the behavior of molecular ionization with high intensity laser pulses.[12,30–32]

RESULTS AND DISCUSSION

Optimal conditions for photoionization with intense fs laser pulses have yet to be established. Here we examine the response of a variety of different molecular systems to test the viability of this approach to increasing the sensitivity of ion-beam induced desorption measurements, and begin to assess the important photoionization mechanisms that yield the largest signals. We examine three classes of molecules including metal oxides, amino acids and polycyclic aromatic hydrocarbons. Detection of these neutral species via postionization opens the possibility of more quantitative measurements compared to SIMS because the desorption step and the ionization step are decoupled. Moreover, the enhanced sensitivity is valuable for chemical imaging experiments where spatial resolution is most often limited by the amount of signal.

We first consider the case of metal oxide systems, a problematic situation for the SIMS approach because of large matrix effects when comparing metal and metal oxide secondary ion intensities. A chemical map of TiO from a Ti integrated circuit on glass is presented in Fig. 2. The image is obtained by monitoring the postionization signal of TiO, generated with 100 fs 800 nm pulses at 1.43×10^{14} W/cm^2, as the ion beam is rastered across the sample surface. A break in the circuit is observed in the left portion of this 225 μm field of view image collected at a 256 × 256 pixel density. When comparing signal intensities in the postionization and positive SIMS spectra (not shown) the TiO:Ti ratio is over a factor of four greater in the former. Taking into consideration that the ionization potential for the oxide[33] is nearly identical to the metal[34] and that the initial monolayer should contain a high concentration of TiO, surface analysis utilizing postionization provides a quantitative representation of the surface composition.

For metal oxide systems, the laser intensity can be increased to the point when the TiO^+ and Ti^+ reach a maximum, saturated value. For organic molecules, however, laser-induced fragmentation eventually begins to reduce the ion intensity even as the laser power is increased to the highest available values. Moreover, there is excess energy deposited into the ion even when utilizing the minimum number of photons required to achieve ionization. These ideas are illustrated below for the excitation of amino acids with 200 nm photons. Amino acids contain a backbone consisting of $COOHCHNH_2$, and excitation through this backbone,[35] or a functional group within the backbone, provides a resonance step for photoionization. The absorption cross section for resonant steps is generally 10^3–10^5 larger than non-resonant steps. Therefore, resonance excitation can provide enhanced detection efficiency at lower laser intensities.

The positive SIMS spectrum of phenylalanine compared to excitation at 200 nm of the desorbed neutral particles is shown in Fig. 3. The spectra were recorded under identical ion-desorption conditions and represent the same number of acquisition cycles. The base peak in the SIMS spectrum, Fig. 3(a), corresponds to Na^+, which is a contaminant in the phenylalanine sample. The two dominant peaks observed, which are characteristic of the compound, are the molecular ion $[M+H]^+$ and loss of carboxylic acid. Moreover, the 'R' group from the amino acid is also observed at *m/z* 91.

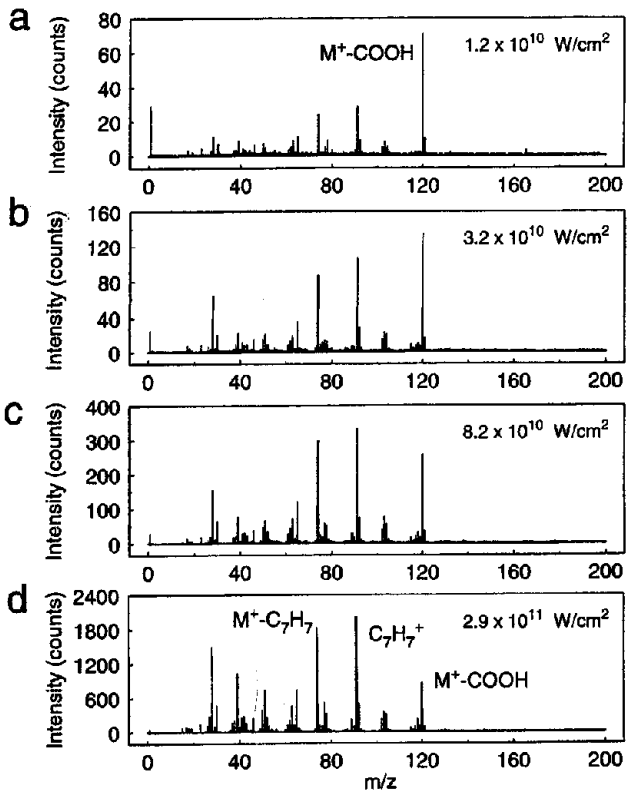

Figure 4. TOF-postionization spectra of phenylalanine taken with 200 nm femtosecond laser pulses at (a) 1.2×10^{10} W/cm^2, (b) 3.2×10^{10} W/cm^2, (c) 8.2×10^{10} W/cm^2 and (d) 2.9×10^{11} W/cm^2.

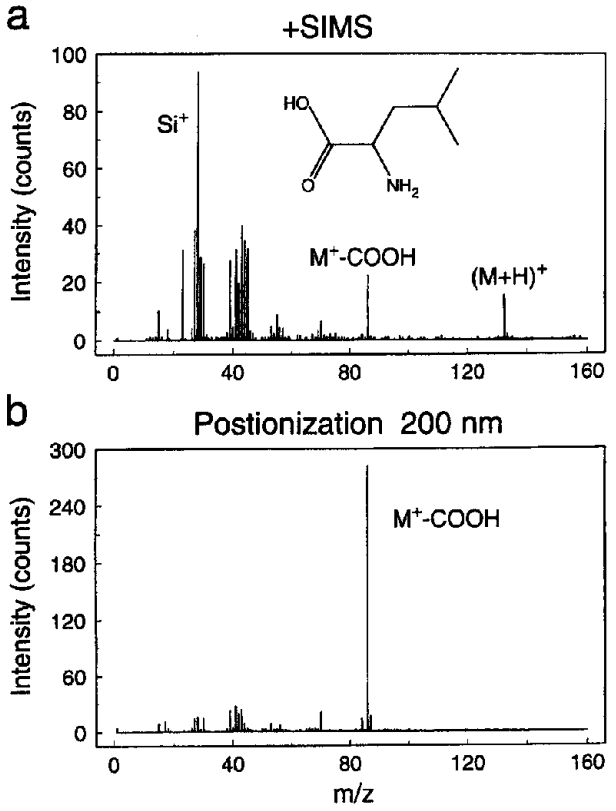

Figure 5. TOF spectra of leucine on Si. (a) +SIMS (b) femtosecond-postionization at 200 nm at $\sim 5 \times 10^{10}$ W/cm^2.

Similar characteristic fragment ions, including the amino acid backbone at *m/z* 74, are present in the postionization spectrum, Fig. 3(b), but the molecular ion is absent.

The lack of molecular ion signal in the postionization data can be caused by a number of factors. The respective distribution of molecular species to fragments may be vastly different for the neutral particles and ions ejected during the desorption process. However, given that there is a substantial molecular ion signal in the SIMS data but essentially none in postionization, a more likely scenario is fragmentation caused by the laser. The application of femtosecond pulses suggests fragmentation through neutral intermediate channels is minimized. The ionization potential of phenylalanine is 8.5 eV.[36] Absorption of two 200 nm photons deposits 3.9 eV of excess energy into the ion. Governed by the selection rules and Frank–Condon factors of the excited and ionic molecular states, the excess energy is partitioned into kinetic energy of the ejected electron and the excited ionic states.

The signal level and degree of fragmentation observed in postionization data are governed by the laser intensity utilized in the experiment. This idea is clearly demonstrated in Fig. 4 where the postionization spectrum of phenylalanine at 200 nm is plotted at increasing laser intensity (Fig. 3(b) is identical to Fig. 4(c)). The highest mass peak observed characteristic of the analyte is the fragment ion at *m/z* 120 corresponding to the loss of COOH. At low laser intensity, Fig. 4(a), the M^+-COOH fragment ion is the base peak in the mass spectrum. As the intensity increases, the degree of fragmentation increases. This observation is consistent with dissociation occurring in the ion. The amino acid backbone and 'R'-group fragment ions change from prominent to the dominant peaks in the spectrum. At high laser intensity, Fig. 4(d), the fragment ion at *m/z* 120 is now a minor mass channel. However, the intensity of this peak is over an order of magnitude larger than at low laser intensity, Fig. 4(a). At laser threshold conditions, two-photon excitation at 200 nm presumably results in fragmentation due to the excess energy deposited into the molecule. As the laser intensity increases, the probability of ionization increases leading to larger signal levels. At high enough intensities, higher order processes become apparent leading to fragmentation in the ion.

The dimension of the laser beam is also a key factor in the observed signal level in postionization experiments. At a fixed laser beam area, increasing the laser power enlarges the geometric volume in which photoionization occurs. This results in a greater observed signal level due to the increased overlap between the photoionization volume and the desorbed particles. In the current experiment, however, the increase in intensity is only possible through focusing of the laser beam. Therefore, the ionization volume increases at the cost of decreasing the laser spot size. These two competing factors eventually result in saturation at a reduced volume, which limits the signal level.

Similar fragmentation pathways are observed for leucine as shown in Fig. 5. The molecular ion adduct (i.e. $[M+H]^+$) can clearly be observed in the positive SIMS spectrum in Fig. 5(a). The other strong peak which can easily be identified as belonging to leucine is the loss of carboxylic acid at *m/z* 86. The postionization spectrum presented in Fig. 5(b), collected under identical ion desorption conditions, greatly differs from the SIMS spectrum. The ionization potential for leucine, at 8.51 eV,[36] is nearly identical to that of phenylalanine. Two-photon excitation at 200 nm potentially deposits up to 3.89 eV of excess energy in the ion. If

this energy is not removed by the departing electron upon ionization, it must be distributed within the ion. As in the case for phenylalanine, the dominant peak in the post-ionization spectrum is assigned to the ammonium ion. This peak, however, is an order of magnitude larger than any characteristic leucine fragments in SIMS. The postionization spectrum was collected at a laser intensity that maximized the signal level, while minimizing fragmentation. The observed fragmentation is presumably due to bond cleavage as a result of excess energy remaining in the ion following photoionization. Trace quantities of the molecular ion are detected, but only at laser threshold conditions.

The lowest ionization energy for amino acids (with the exception of tyrosine, tryptophan, and sulfur-containing methionine and cysteine) is associated with removal of an electron from the nitrogen lone pair orbital of the amine. For phenylalanine, however, it is difficult to distinguish whether the lowest energy transition corresponds to ionization from the nitrogen lone pair or the aromatic phenyl π orbitals.[36] Excitation of phenylalanine at 200 nm may lead to absorption through either the phenyl[39] or amine group.[35] The route of excitation may determine from which state ionization occurs, and the resulting final state populated in the ion may govern the degree of fragmentation observed in the spectrum. For instance, the phenyl group has numerous normal modes to redistribute excess energy (thus reducing fragmentation) as compared to the amine group. In the current postionization study for phenylalanine and leucine, it is not possible to determine whether fragmentation is a result of the excess energy deposited in the ion or the final state populated.

Pump-probe experiments will differentiate between these two scenarios. Excitation at 200 nm followed by ionization with 400 nm photons will deposit only 0.8 eV of excess energy in the ion. Comparing these results to those obtained for the excitation and ionization of phenylalanine at 267 nm should help resolve the issue. In both cases, two-photon excitation corresponds to the absorption of 9.3 eV of energy. The difference, however, is the path of excitation. Excitation at 200 nm leads to the absorption through the amine group (also the phenyl group in phenylalanine), whereas absorption of 267 nm photons results in excitation of the aromatic π orbitals on phenylalanine, not present in leucine.

To fully understand the results obtained in this study, it is crucial to separate the desorption and photoionization steps. From preliminary results for dopamine, however, it is suggested that the lack of molecular ion signal in post-ionization experiments for molecules with labile chains may be attributed to the photoionization of internally 'hot' sputtered molecules.[38] The molecular ion signal is present in SIMS experiments, but absent during postionization at 267 nm. In the gas phase data, fragmentation occurs, but the molecular ion is a dominant peak in the spectrum.

Postionization of conjugated systems exhibits a distinctly different behavior. The +SIMS and postionization spectra of pyrene butyric acid (PBA) bound to silver beads is shown in Fig. 6. The spectra are recorded under identical ion desorption conditions. The strong Si peak observed in SIMS is attributed to the substrate on which the beads are supported. The contribution from PBA is a minor component of the spectrum, with the dominant feature assigned to the loss of the alkyl chain [i.e. $M^+-(CH_2)_2COOH$] at *m/z* 215. Excitation at 267 nm of the desorbed neutrals leads to a spectrum dominated by features belonging to PBA. The spectrum is recorded at low laser power to minimize

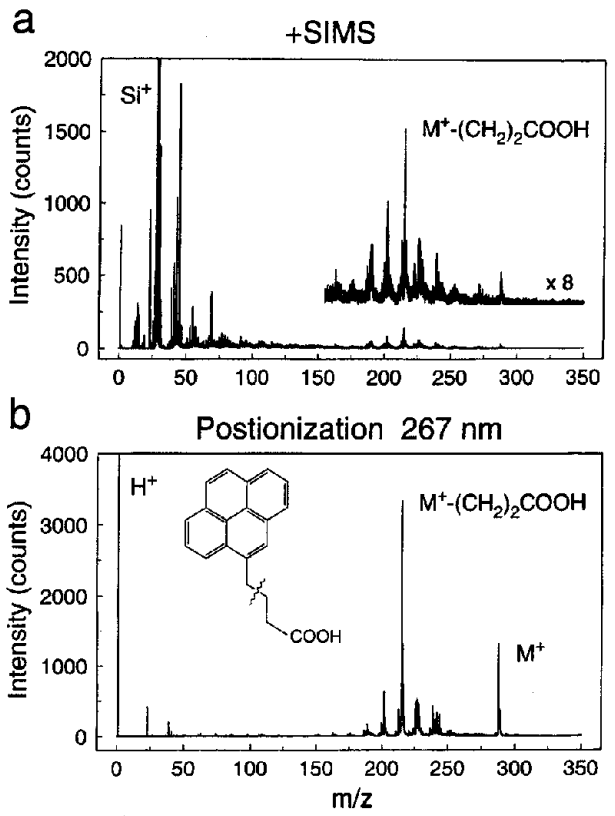

Figure 6. TOF spectrum of pyrene butyric acid (PBA) desorbed from Ag beads. (a) +SIMS (b) femtosecond-postionization at 200 nm. The molecular ion and primary fragment ion in the postionization mass spectrum correspond to *m/z* 288 and 215, respectively.

fragmentation. A reduction in laser power does not change the observed ratio of the 215:M^+, only a decrease in signal level. Even at these laser conditions the postionization signal from the molecules of interest is over an order of magnitude larger when compared to +SIMS. At higher laser powers the degree of fragmentation increases, but so does the signal corresponding to PBA. Signal from the Si substrate is also observed at these laser conditions.

It is evident from the SIMS spectrum, Fig. 6(a), that only a small fraction of molecular ions are desorbed during ion bombardment. Assuming the relative distributions (i.e. fragments to molecular species) are similar for the desorbed ions and neutrals of PBA, excitation at 267 nm initiates little or no fragmentation. To the best of our knowledge the ionization potential for PBA has not been determined. The ionization potential for pyrene, however, measured using two-laser photoionization is 7.426 eV.[39] Assuming the value for PBA is not vastly different, absorption of two photons at 267 nm deposits roughly 2 eV of excess energy into the molecule. In these systems, the C–H bonds are the weakest. Therefore, fragmentation generally consists of H atom loss, which makes the assignment of these features straightforward. Moreover, fragmentation of the ring requires the dissociation of two C–C bonds. These ideas have been confirmed in earlier work reported on the conjugated system benzo[a]pyrene.[15] In postionization experiments utilizing UV excitation, minimal fragmentation is observed. For PBA, Fig. 6(b), the dominant fragment peaks in the postionization spectrum correspond to dissociation along the alkyl chain. Until gas phase experiments are performed, it will remain unclear whether the fragmen-

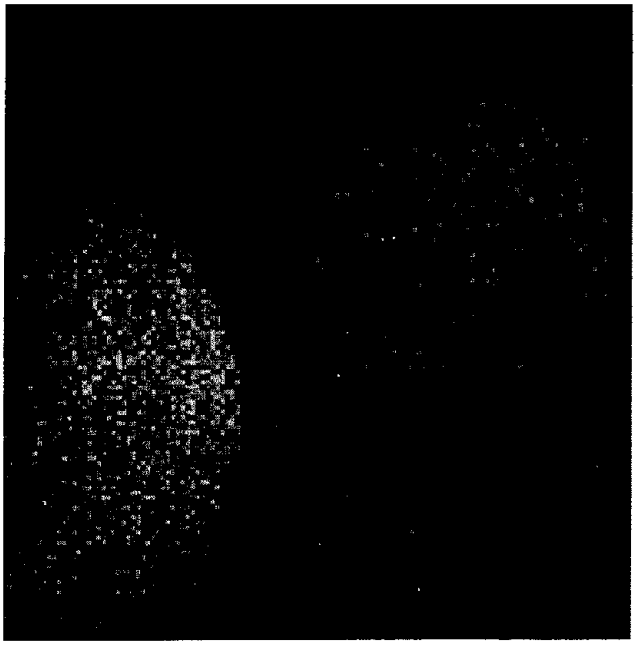

Figure 7. Postionization image of PBA^+ desorbed from Ag beads using 60 ns (2 nA) ion gun pulses with 40 shots per pixel (2.2×10^{12} Ga^+ ions/cm^2). The PBA molecules are ionized with 267 nm, 250 fs laser pulses at a laser power of 1.4×10^{11} W/cm^2. The 128 pixel × 128 pixel image was collected from a 150 μm × 150 μm area.

tation occurs during sputtering or the photoionization step. Substantial fragmentation, however, is observed in the +SIMS spectrum.

An image formed by detection of desorbed neutral PBA molecules is shown in Fig. 7. The field of view is 150 μm and the image is collected at a resolution of 128 × 128 pixels. It is clearly observed that the molecular ion signal is localized to the Ag beads. Signal from Ag is not present because the sample is deposited in multi-layers on the beads. The laser power could also be increased to vastly decrease the acquisition time. The degree of fragmentation becomes greater, but the signal level in the *m/z* 215 channel increases. Degradation of image quality due to changes in instrumental conditions eventually occurs over time. This fact reinforces the need for fast and highly sensitive detection techniques. The image of PBA in Fig. 7 presents the clear potential postionization offers to the identification of molecular species on the micron scale.

CONCLUSION

In this work, we have described the instrumental parameters that are critical in postionization studies and their relevance to chemical imaging. Incorporating femtosecond laser pulses has eliminated losses of molecular species through the neutral fragmentation channels that have plagued experiments utilizing nanosecond excitation. Non-resonant MPI can best describe the results presented above, but at high laser intensities alternative ionization mechanisms (i.e. tunneling and barrier suppression ionization) become operative. The full potential of ionization through these mechanisms has yet to be realized. Current work in our laboratory is exploring these avenues. A major advantage to the new Ti:sapphire laser system is the kHz repetition rates, which greatly reduces acquisition time over conventional nanosecond laser systems. As demonstrated here, matrix effects are diminished in postionization studies leading to a better representation of the true surface composition during analysis.

Acknowledgements

The authors appreciate the financial support of the National Science Foundation and the National Institutes of Health. In addition, we are grateful for the advice of Philippe Bado of Clark MXR and an NSF STTC Award involving the two laboratories.

REFERENCES

1. A. Benninghoven, F. G. Rudenauer and H. W. Werner, *Secondary ion mass spectrometry, basic concepts, instrumental aspects, applications, and trends*, Wiley-Interscience, New York (1987).
2. D. L. Pappas, D. M. Hrubowchak, M. H. Ervin and N. Winograd, *Science* **243,** 64 (1989).
3. D. M. Hrubowchak, M. H. Ervin, M. C. Wood and N. Winograd, *Anal. Chem.* **63,** 1947 (1991).
4. M. C. Wood, Y. Zhou, C. L. Brummel and N. Winograd, *Anal. Chem.* **66,** 2425 (1994).
5. N. Winograd, *Anal. Chem.* **65,** 622A (1993).
6. U. Schuhle, J. B. Pallix and C. H. Becker, *J. Am. Chem. Soc.* **110,** 2323 (1988).
7. H. S. Kilic, K. W. D. Ledingham, C. Kosmidis, T. McCanny, R. P. Singhal, S. L. Wang, D. J. Smith, A. J. Langley and W. Shaikh, *J. Phys. Chem. A* **101,** 817 (1997).
8. K. W. D. Ledingham, C. Kosmidis, S. Georgiou, S. Couris and R. P. Singhal, *Chem. Phys. Lett.* **247,** 555 (1995).
9. M. A. Duncan, T. G. Dietz and R. E. Smalley, *Chem. Phys.* **44,** 415 (1979).
10. D. A. Gobeli, J. J. Yang and M. A. El-Sayed, *Chem. Rev.* **85,** 529 (1985).
11. C. Grun, C. Weickhardt and J. Grotemeyer, *J. Eur. Mass Spectrom.* **2,** 197 (1996).
12. K. F. Willey, C. L. Brummel and N. Winograd, *Chem. Phys. Lett.* **267,** 359 (1997).
13. M. A. Terhorst, R. Möllers, E. Niehuis and A. Benninghoven, *Surf. Interface Anal.* **18,** 824 (1992).
14. R. Möllers, M. Terhorst, E. Niehuis and A. Benninghoven, *Org. Mass Spectrom.* **27,** 1393 (1992).
15. C. L. Brummel, K. F. Willey, J. C. Vickerman and N. Winograd, *Int. J. Mass Spectrom. Ion Processes* **143,** 257 (1995).
16. R. M. Braun, P. Blenkinsopp, S. J. Mullock, C. Corlett, K. F. Willey, J. C. Vickerman and W. Winograd, *Rapid Commun. Mass. Spectrom.* **12,** 1246 (1998).
17. L. K. Chau and M. D. Porter, *Chem. Phys. Lett.* **167,** 198 (1990).
18. P. Maine, D. Strickland, P. Bado, M. Passot and G. Mourou, *IEEE J. Quantum, Electron* **QE-24,** 398 (1988).
19. G. Vaillancourt, T. B. Norris, J. S. Coe, P. Bado and G. A. Mourou, *Opt. Lett.* **15,** 317 (1990).
20. F. Salin, J. Squier, G. Mourou and G. Vaillancourt, *Opt. Lett.* **16,** 1964 (1991).
21. M. A. Dugan, M. L. Pacholski, K. F. Willey, R. M. Braun and N. Winograd, in *Resonance Ionization Spectroscopy 1996: Eighth International Symposium*, N. Winograd and J. E. Parks (Eds.), AIP Press, Woodbury, New York (1997).
22. H. C. Captain and M. M. Mourning, *Optics & Photonics News* **5,** 20 (1994).
23. V. S. Letokhov, *Laser Photoionziation Spectroscopy*, Academic Press, New York (1987).
24. P. Zoller and P. Lambropoulos, *J. Phys. B: At. Mol. Phys.* **13,** 69 (1980).
25. L. V. Keldysh, *Sov. Phys. JETP* **20,** 307 (1965).
26. L. A. Lompre, G. Mainfray, C. Manus, S. Repoux and J. Thebault, *Phys. Rev. Lett.* **36,** 949 (1976).
27. F. A. Ilkov, J. E. Decker and S. L. Chin, *J. Phys. B: At. Mol. Opt. Phys.* **25,** 4005 (1992).
28. S. Augst, D. D. Meyerhofer, D. Strickland and S. L. Chin, *J. Opt. Soc. Am. B* **8,** 858 (1991).
29. S. Augst, D. Strickland, D. D. Meyerhofer, S. L. Chin and J. H. Eberly, *Phys. Rev. Lett.* **63,** 2212 (1989).
30. C. H. Becker and J. S. Hovis, *J. Vac. Sci. Technol. A* **12,** 2352 (1994).
31. T. D. G. Walsh, F. A. Ilkov, J. E. Decker and S. L. Chin, *J. Phys. B: At. Mol. Opt. Phys.* **27,** 3767 (1994).

32. M. J. DeWitt and R. J. Levis, *J. Chem. Phys.* **102,** 8670 (1995).
33. A. D. Sappey, G. Eiden, J. E. Harrington and J. C. Weisshaar, *J. Chem. Phys.* **90,** 1415 (1989).
34. R. H. Page and C. S. Gudeman, *J. Opt. Soc. Am. B* **7,** 1761 (1990).
35. *Handbook of Spectroscopy*, Vol. II, J. W. Robinson (Ed.), CRC Press, Cleveland (1974).
36. S. Campell, J. L. Beauchamp, M. Rempe and D. L. Lichtenberger, *Int. J. Mass Specrom. Ion Processes* **117,** 83 (1992).
37. R. M. Silverstein, G. C. Bassler and T. C. Morrill, *Spectrometric Identification of Organic Compounds*, 5th edition, Wiley, New York (1991).
38. K. F. Wiley, C. L. Brummel and N. Winograd, in *Secondary Ion Mass Spectrometry (SIMS X)*, A. Benninghoven, B. Hagenhoff and H. W. Werner (Eds), Wiley, Chichester (1996).
39. J. W. Hager and S. C. Wallace, *Anal. Chem.* **60,** 5 (1988).